

Nonlinear ionization control by temporally shaped fs+ps double-pulse sequence on ZnO

Weiyi Yin (尹唯一)¹, Juan Song (宋娟)², Xiangyu Ren (任翔宇)¹, Qian Yao (姚倩)¹, Xian Lin (林贤)¹, and Ye Dai (戴晔)^{1*}

¹Department of Physics, Shanghai University, Shanghai 200444, China

²School of Material Science and Engineering, Jiangsu University, Zhenjiang 212013, China

*Corresponding author: yedai@shu.edu.cn

Received July 12, 2022 | Accepted August 15, 2022 | Posted Online September 13, 2022

We designed a femtosecond (fs) + picosecond (ps) double-pulse sequence by using a Mach-Zehnder-like apparatus to split a single 120 fs pulse into two sub-pulses, and one of them was stretched to a width of 2 ps by a four-pass grating system. Through observing the ripples induced on the ZnO surface, we found the ionization rate appeared to be higher for the sequence in which the fs pulse arrived first. The electron rate equation was used to calculate changes of electron density distribution for the sequences with different delay times. We suggest that using a temporally shaped fs+ps pulse sequence can achieve nonlinear ionization control and influence the induced ripples.

Keywords: ZnO; ultrafast double-pulse sequence; ripple; temporal shaping; nonlinear ionization.

DOI: [10.3788/COL202321.021602](https://doi.org/10.3788/COL202321.021602)

1. Introduction

ZnO is one of the well-known near ultraviolet luminescence semiconductors owing to its wide band gap of 3.4 eV and large exciton binding energy of 60 mV, and its surface nanostructures have been reported to improve the photoelectron conversion efficiency^[1,2]. Therefore, nanostructured ZnO is a promising material for high-power emitting devices and photodetector applications^[3]. Among the methods of nanostructure preparation on ZnO, femtosecond (fs) laser irradiation has been regarded as an efficient technique for large-scale precision processing by virtue of flexible non-contact one-step direct writing capability^[4,5].

In recent years, improving the fs laser processing efficiency has attracted more and more attention^[6–8]. Previous studies usually focused on adjusting laser parameters such as pulse energy, pulse number, and pulse width. Nowadays, the use of the double-pulse sequence has become an emerging strategy to improve processing efficiency^[9] and quality^[10], because it can precisely control the material ionization process by adjusting delay time, energy ratio, and polarization state^[11]. For example, Barberoglou *et al.* reported the capability of double-fs pulses to switch the induced structures from low to high spatial frequency ripples on ZnO^[12]. Our group has also used double-fs pulse sequence irradiation to study the mechanism of nanograting formation by adjusting two sub-pulses' delay time [from sub-picoseconds (ps) to hundreds of ps] in SiO₂^[13,14]. In addition, there are some extended schemes for the double-pulse sequence. Höhm *et al.* compared the experimental results of

800 nm + 400 nm double-fs pulses on different materials and proposed a wavelength-dependent plasma generation mechanism^[15]. Miyamoto *et al.* used a coaxial combination of fs laser and continuous-wave laser to explore more efficient ways to enhance the ionization process in glass. Because the characteristics of both types of lasers can be fully taken into account for material ionization, the processing speed was about 500 times higher than that of ordinal methods^[16]. These studies have provided a range of evidence for double-pulse sequence irradiation improving the processing efficiency. However, for the ordinal double-fs pulse sequence, the pulse width is so short that the interaction between two sub-pulses is only indirect through the induced excitons or defects in the materials. As far as for the sequence of two short-long sub-pulses [e.g., fs + microseconds (μs)], their widths differ greatly, so the long pulse far exceeds the lifetime of the electrons excited by the short pulse, leading to the inefficiency of energy deposition. In addition, the long pulse easily causes thermal effects and melts the nanostructures^[17]. Based on an idea of taking advantage of direct interaction between two sub-pulses for nonlinear ionization control, we propose using the fs+ps double-pulse sequence (FPDPS) to improve the processing efficiency.

In this Letter, we generated a 120 fs + 2 ps double-pulse sequence by a Mach-Zehnder-like apparatus, which included a four-path grating system. The induced ZnO surface ripples showed obvious structural difference through changing the delay times between the two sub-pulses. This is because the electron density excited by different FPDPSs made a strong effect on formation of surface structure. The experimental result agrees

with the assumption based on the calculation by using the electron rate equation. This research contributes to a deep understanding of the role of the temporal shaping double-pulse sequence in laser material processing.

2. Experiment

A commercial chirped pulse Ti:sapphire regenerative laser amplifier system (Spitfire Pro, Spectra-Physics Co.) was employed to obtain a linearly polarized fs pulse train with a wavelength of 780 nm, a pulse width of 120 fs, and a repetition rate of 1 kHz. The output laser was split into two arms by a Mach-Zehnder-like apparatus, as shown in Fig. 1(a). A grating (600 lines/mm) was inserted in the ps arm to build a four-pass system to separate the spectra of this sub-pulse for temporal broadening^[18,19]. In the four-pass design, the optical path is always incident to the grating by precisely adjusting two retroreflectors mounted on guide rails, and the spatial intensity distribution of the temporally stretched ps pulse basically remained a Gaussian profile, as shown in Fig. 1(c). The intensity distributions were measured by a laser beam profile (SP503U, Ophir-Spiricon). The major axes of the spot in Figs. 1(b) and 1(c) are 3.9 mm and 4.2 mm, respectively. The two spots will be limited to the same size by a shutter with an aperture of 3 mm. In this apparatus, the double-pulse sequence was set to 120 fs+2 ps, which was measured by an autocorrelator (Pulse Scout, Spectra-Physics). The delay time τ between these two sub-pulses was motor controlled from -80 to 80 ps by a delay line (in the fs arm) with a resolution of 16.7 fs. Figure 1(d) shows three delay times of this FPDPS. Specifically, the fs pulse arriving prior to the ps pulse is defined as a negative delay. Neutral density filters

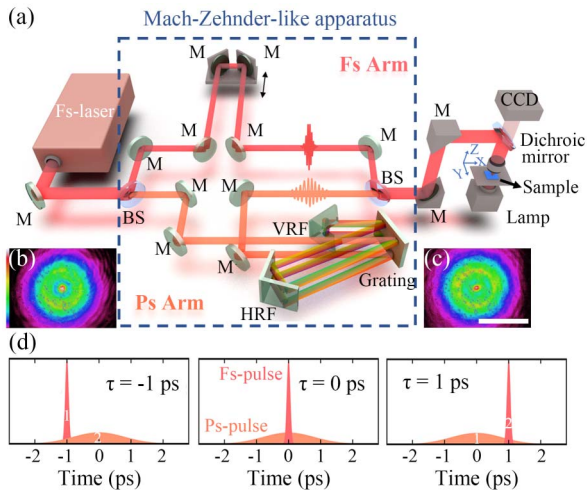


Fig. 1. (a) Schematic diagram of experimental setup based on a Mach-Zehnder-like apparatus. M, mirror; BS, beam splitter; HRF, horizontal retroreflector; VRF, vertical retroreflector. (b) Spatial light intensity distributions of fs pulse. (c) Spatial light intensity distributions of temporally shaped ps pulse. The scale bar is 3 mm. (d) Schematic diagram of temporal delays between two sub-pulses.

and a half-wave plate were set to adjust the pulse energy and polarization in two arms, respectively. The generated FPDPSs with the same polarization were focused onto the surface of ZnO through a $5\times$ objective (NA = 0.15, Nikon ECLIPSE 80i). The sample was placed on a computer-controlled XYZ stage. The laser-irradiated surface regions were inspected by scanning electron microscopy (SEM) (Hitachi, SU5000).

3. Result and Discussion

A constant number ($N = 25$) of FPDPSs were used to irradiate the ZnO surface with each sub-pulse energy of $0.72 \mu\text{J}$ (the spot diameter is about $14 \mu\text{m}$, corresponding to the fluence of $0.45 \text{ J}/\text{cm}^2$), and then we found the laser-induced periodic surface structure (LIPSS, ripples) appeared accordingly. Generally, these ripples can be divided into two types: near-wavelength LIPSS with low-spatial-frequency (LSFL) and sub-wavelength LIPSS with high-spatial-frequency (HSFL). In our experiment, both of these ripples have been observed. In Fig. 2, we plot the trend of the ripple area over the delay time. With an increase of the delay time, the ripple area gradually decreases until no structure appears in the irradiated region. A series of SEM pictures of nanostructures corresponding to different delay times are shown as the insets in Fig. 2.

In the irradiation with a negative delay of $\tau = -0.32$ ps, both types of ripples can be observed, and they covered an area of about $127 \mu\text{m}^2$. The LSFL with a period of 620–650 nm formed in the area center, and the HSFL with a period of 220–250 nm appeared at the outer region. The orientations of both LSFL and HSFL were perpendicular to the laser polarization. On the other side with a positive delay of $\tau = +0.32$ ps, the ripple area was only about $53 \mu\text{m}^2$, much smaller than the negative delay case. Next, we continued increasing the delay time to $\tau = \pm 1$ ps. The area difference between these two cases was more obvious. When $\tau = -1$ ps, the induced ripple area increased fourfold over the one for $\tau = +1$ ps. In addition, both HSFL and LSFL could be observed at $\tau = -1$ ps, while the positive delay irradiation only

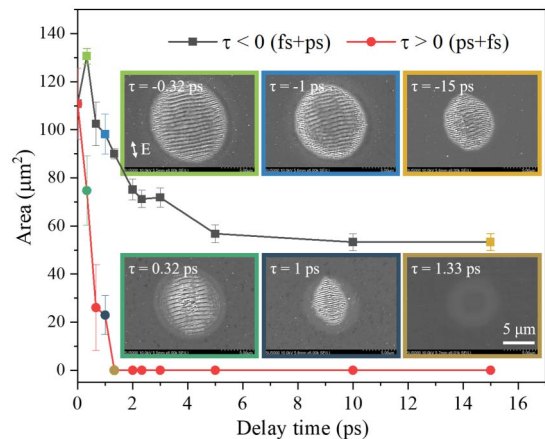


Fig. 2. Induced ripple areas over the delay times. The markers in two curves correspond to different color blocks for the SEM insets.

produced HSFL. Previous studies claimed that the transition between HSFL and LSFL strongly depends on pulse fluence^[12,20]. For example, Barberoglou *et al.*^[12] found that the LSFL could not form on ZnO when the fluence was below 0.55 J/cm², however, the HSFL could be observed. That indicates that the generation of LSFL needs a higher fluence compared to the HSFL. As the delay time continued increasing, the ripple area gradually contracted until it cannot be observed anymore at $\tau = +1.33$ ps. However, on the other side of negative delay time, the ripples still could form even at $\tau = -80$ ps (not displayed in Fig. 2). Therefore, either the ripple area or the induced structure type reflects that a relative high processing efficiency can be achieved when using a negative delay FPDPS. Moreover, we also clearly realized that the formation of the nanostructure was closely related to the excited electron density^[13,14]. These phenomena possibly imply that the arrival order of sub-pulses in single FPDPS could make a significant effect on the electron density control.

We used the electron rate equation to calculate the maximum density (ρ) induced by an FPDPS^[21,22]:

$$\frac{\partial \rho}{\partial t} = \frac{1}{n_0^2} \frac{\sigma}{E_g} \rho |E|^2 + \frac{\beta_K |E|^{2K}}{K \hbar \omega} - \gamma \rho^3 - \frac{\rho}{\tau_R}, \quad (1)$$

where avalanche ionization, multiphoton absorption, Auger recombination, and electron lifetime are involved, respectively. In addition, inverse bremsstrahlung cross-section σ and laser light intensity E are expressed as

$$\sigma = \frac{e^2 \tau_e}{cn_0 \epsilon_0 m_{\text{eff}} (\omega^2 \tau_e^2 + 1)}, \quad (2)$$

$$E = \sqrt{\frac{F}{\tau_1 \sqrt{\pi/2}}} e^{-\frac{r^2}{\tau_1^2}} \cdot e^{-\frac{t^2}{\tau_1^2}} + \sqrt{\frac{F}{\tau_2 \sqrt{\pi/2}}} e^{-\frac{r^2}{\tau_2^2}} \cdot e^{-\frac{(t-\tau)^2}{\tau_2^2}}. \quad (3)$$

In Eq. (1), K is the number of instantaneous absorbed photons required for the band transition, and three-photon absorption is considered here. Other parameters are described in Table 1.

Figure 3(a) summarizes the maximum electron density over radial position r and delay time τ . On the side of negative delay, a large area of high concentration electrons can be excited. As an example, Fig. 3(b) shows two curves of electron density distributions corresponding to the two cases of $\tau = \pm 1$ ps. In the case of $\tau = +1$ ps, following the incident Gaussian intensity distribution, the electron density decreases quickly along the radial position. But, different from the front, the case of negative delay shows a higher flat top, indicating higher energy absorption efficiency. The difference between these two electron density distributions might result from different avalanche ionization rates, because the first arrival pulse could affect the generation number of seed electrons. As for the reason for different structural types, it is generally accepted that LSFL arises from the interference of incident radiation with a surface electromagnetic wave, which might include the excitation of surface plasmon polaritons (SPPs)^[28]. To induce the LSFL according to the SPP-based

model, two conditions need to be satisfied^[15]: the electron density is high enough to instantly turn the transparent ZnO surface into a metallic state, and the incident light interferes with

Table 1. Parameters for ZnO in Electron Density Rate Equation.

Symbol	Description	Value
n_0	Original material index	2
E_g	Band gap	3.46 eV
β	Multiphoton absorption coefficient	0.016 cm ³ /GW ² ^[23]
ω	Light frequency for 780 nm	$c/780$ nm
γ	Auger recombination coefficient	0.96×10^{-39} cm ⁶ /s ^[24]
τ_R	Electron hole recombination time	2.8 ns ^[25]
c	Speed of light	299,792,458 m/s
ϵ_0	Permittivity of vacuum	8.85×10^{-12} F/m ^[26]
τ_e	Electron collision time	46 fs ^[27]
m_{eff}	Effective electron mass	$0.28m_0$ ^[26]
F	Incident fluence	0.45 J/cm ²
ω_0	Spot radius	5.5 μ m
τ_1	Parameters related to ps pulse	$\tau_{\text{ps}}/2\sqrt{2 \ln 2}$
τ_2	Parameters related to fs pulse	$\tau_{\text{fs}}/2\sqrt{2 \ln 2}$
$\tau_{\text{fs}}, \tau_{\text{ps}}$	Pulse width	120 fs, 2 ps
r	Radical position	-10 to 10 μ m

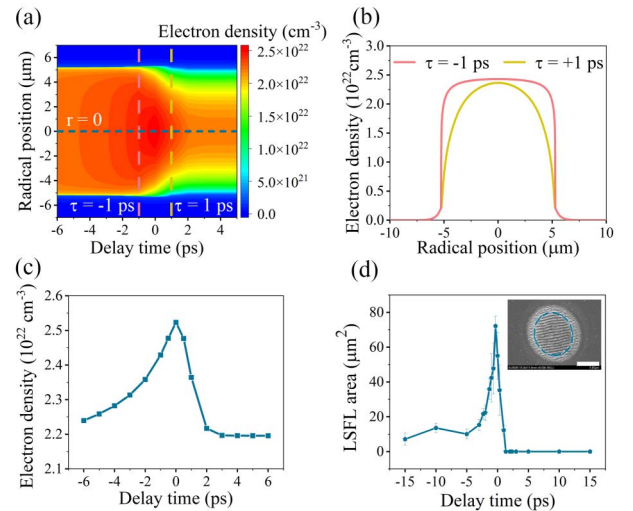


Fig. 3. (a) Maximum electron density at different radial positions and delay times. (b) The electron density distributions corresponding to $\tau = \pm 1$ ps, respectively. (c) The area center electron density over delay times. (d) Dependence of LSFL area on delay time. The insert shows an SEM picture of the LSFL covered area. The scale bar is 5 μ m.

the electromagnetic field of SPP. Dufft *et al.* reported that the ZnO surface would turn into a metallic state if the generated electron density exceeds $\sim 5 \times 10^{21} \text{ cm}^{-3}$ ^[29]. In our case, the negative delay FPDPS may produce $\rho \gg 5 \times 10^{21} \text{ cm}^{-3}$, which is conducive to the excitation of SPP and the formation of LSFL. The formation mechanism of HSFL is controversially discussed. One point of view is that the interference between the generated second harmonic and the surface electromagnetic wave gives rise to HSFL^[29,30]. As a result, the areas of HSFL can be larger than those covered by LSFL.

Figure 3(c) shows the maximum electron density at the area center ($r = 0$) with various delay times. The decreasing trend of electron density over delay time is basically consistent with the decreasing trend of the induced LSFL area in Fig. 3(d), although some HSFLs formed around the center. It is known that the total ripple area consisting of HSFL and LSFL depended closely on the electron density distribution^[31]. Both theoretical and experimental results clearly prove that the FPDPS can affect the excited electron density distribution, and the first arriving fs pulse may cause a higher ionization rate.

As for the mechanism of the controlling ionization rate on the ZnO surface by temporally shaped FPDPSs, we proposed the following physical scenario: when an ultrashort pulse is focused on the ZnO surface, in the irradiated area, the valence band electron instantaneously absorbs three photons to transit to the conduction band. When the sub-pulse energy is constant, the multiphoton absorption is more intensive in the case of fs pulses first arriving due to the relatively higher peak power, resulting in more free electrons being excited in a larger area, as shown in Fig. 4(a). Very shortly, some of the excited electrons may behave as seeds to efficiently absorb the ps pulse energy via the inverse bremsstrahlung effect. This electron acceleration process will lead to seed avalanche ionization and further increase the electron density^[32]. After a number of FPDPSs accumulation, a ripple area consisting of LSFL and HSFL forms. However, it is important to point out that an increasing delay time will greatly weaken the seed avalanche ionization between two sub-pulses

in an FPDPS. Therefore, the ripple area decreased with the delay time increasing, as shown in Fig. 2. Figure 4(b) shows a diagram with the ps pulse arriving first. As the original fs pulse was temporally stretched to lower its peak power, the excited electron density possibly becomes too small to support the growth of LSFL or HSFL in the whole irradiated area. The above assumption presents a dynamic nonlinear ionization control in material processing.

4. Conclusion

In this study, we used a home-built Mach–Zehnder-like apparatus, which included a temporally shaped system to obtain a 120 fs + 2 ps double-pulse sequence. These sequences with two sub-pulses energy ratio of 1:1 were irradiated on the ZnO surface to induce ripples. We found that the arrival order of sub-pulses in single FPDPS could make a difference on the formation of LSFL or HSFL. This selection possibly associates with the excited electron density. With the calculation using an electron rate equation, the FPDPS in which the fs pulse first arrives could excite the higher electron density because strong seed avalanche ionization is easier to trigger shortly in irradiation of the second ps pulse. That nonlinear ionization process elongates the photon–electron interaction time and promotes the energy absorption efficiency. We suggest that this temporally shaped FPDPS provides a new method to enhance pulse energy deposition in material processing.

Acknowledgement

This work was financially supported by the National Natural Science Foundation of China (Nos. 12274280, 11774220 and 11974147).

References

- Q. Li, H. Shi, C. Luo, Z. Fan, H. Wang, L. Zhang, and Y. Liu, "Micropattern-assisted absorption enhancement and wettability surface on ZnO via single femtosecond laser beam tailoring," *Opt. Laser Technol.* **150**, 107979 (2022).
- J. Pan, T. Jia, X. Jia, D. Feng, S. Zhang, Z. Sun, and J. Qiu, "Infrared femtosecond laser-induced great enhancement of ultraviolet luminescence of ZnO two-dimensional nanostructures," *Appl. Phys. A* **117**, 1923 (2014).
- J. Theerthagiri, S. Salla, R. A. Senthil, P. Nithyadharani, A. Madankumar, P. Arunachalam, T. Maiyalagan, and H.-S. Kim, "A review on ZnO nanostructured materials: energy, environmental and biological applications," *Nanotechnology* **30**, 392001 (2019).
- T. Jiang, S. Gao, Z. Tian, H. Zhang, and L. Niu, "Fabrication of diamond ultra-fine structures by femtosecond laser," *Chin. Opt. Lett.* **18**, 101402 (2020).
- X. Jia, T. Jia, L. Ding, P. Xiong, L. Deng, Z. Sun, Z. Wang, J. Qiu, and Z. Xu, "Complex periodic micro/nanostructures on 6H-SiC crystal induced by the interference of three femtosecond laser beams," *Opt. Lett.* **34**, 788 (2009).
- L. Jiang, A. Wang, B. Li, T. Cui, and Y. Lu, "Electrons dynamics control by shaping femtosecond laser pulses in micro/nanofabrication: modeling, method, measurement and application," *Light Sci. Appl.* **7**, 17134 (2018).
- Z. Guo, K. Hu, T. Cao, S. Liu, J. Yan, Z. Li, Q. Xu, P. B. Corkum, and J. Peng, "Energy deposition and incubation effects of nonlinear absorption of ultrashort laser pulses in dielectrics," *Opt. Express* **30**, 10317 (2022).

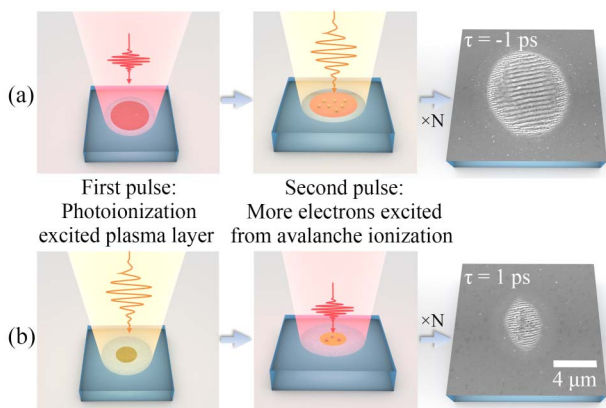


Fig. 4. Schematic diagram of electron excitation and energy absorption during irradiation of different FPDPSs. (a) The fs pulse arrives first. (b) The ps pulse arrives first.

8. Y. Zhang, Q. Jiang, M. Long, R. Han, K. Cao, S. Zhang, D. Feng, T. Jia, Z. Sun, J. Qiu, and H. Xu, "Femtosecond laser-induced periodic structures: mechanisms, techniques, and applications," *Opto-Electron Sci.* **1**, 220005 (2022).
9. Z. Lin, L. Ji, and M. Hong, "Enhancement of femtosecond laser-induced surface ablation via temporal overlapping double-pulse irradiation," *Photonics Res.* **8**, 271 (2020).
10. S. A. Jalil, J. Yang, M. ElKabbash, S. C. Singh, and C. Guo, "Maskless formation of uniform subwavelength periodic surface structures by double temporally-delayed femtosecond laser beams," *Appl. Surf. Sci.* **471**, 516 (2019).
11. Y. Li, J. Hu, W. Liu, J. Yin, and J. Lu, "High period frequency LIPSS emerging on 304 stainless steel under the irradiation of femtosecond laser double-pulse trains," *Chin. Opt. Lett.* **19**, 123801 (2021).
12. M. Barberoglou, D. Gray, E. Magoulakis, C. Fotakis, P. A. Loukakos, and E. Stratakis, "Controlling ripples' periodicity using temporally delayed femtosecond laser double pulses," *Opt. Express* **21**, 18501 (2013).
13. H. Wang, J. Song, Q. Li, X. Zeng, and Y. Dai, "Formation of nanograting in fused silica by temporally delayed femtosecond double-pulse irradiation," *J. Phys. D* **51**, 155101 (2018).
14. W. Zhang, Q. Zhai, J. Song, K. Lou, Y. Li, Z. Ou, Q. Zhao, and Y. Dai, "Manipulation of self-organized nanograting for erasing and rewriting by ultrashort double-pulse sequences irradiation in fused silica," *J. Phys. D* **53**, 165106 (2020).
15. S. Höhm, A. Rosenfeld, J. Krüger, and J. Bonse, "Laser-induced periodic surface structures on zinc oxide crystals upon two-colour femtosecond double-pulse irradiation," *Phys. Scr.* **92**, 034003 (2017).
16. N. Miyamoto, Y. Ito, C. Wei, R. Yoshizaki, A. Shibata, I. Nagasawa, K. Nagato, and N. Sugita, "Ultrafast internal modification of glass by selective absorption of a continuous-wave laser into excited electrons," *Opt. Lett.* **45**, 3171 (2020).
17. N. Casquero, Y. Fuentes-Edfuf, R. Zazo, J. Solis, and J. Siegel, "Generation, control and erasure of dual LIPSS in germanium with fs and ns laser pulses," *J. Phys. D* **53**, 485106 (2020).
18. Q. Li, W. Li, W. Chu, Y. Cao, W. Zhang, H. Ma, Z. Jin, and Y. Dai, "Effect of spatio-temporal coupling on ultrafast laser direct writing in glass," *Chin. Opt. Lett.* **17**, 081402 (2019).
19. X. Tang, Y. Li, Y. Sun, Q. Zhai, H. Ma, and Y. Dai, "Temporally chirped femtosecond pulse laser non-reciprocal writing on the silicon," *Appl. Phys. A* **127**, 135 (2021).
20. X. Shi and X. Xu, "Laser fluence dependence of ripple formation on fused silica by femtosecond laser irradiation," *Appl. Phys. A* **125**, 256 (2019).
21. J. Song, W. Tao, H. Song, M. Gong, G. Ma, Y. Dai, Q. Zhao, and J. Qiu, "Laser-induced periodic surface structures on 6H-SiC single crystals using temporally delayed femtosecond laser double-pulse trains," *Appl. Phys. A* **122**, 341 (2016).
22. L. Jiao, D. Kong, X. Zhang, H. Wang, Y. Dai, and J. Song, "Ripple period adjustment on SiC surface based on electron dynamics control and its polarization anisotropy," *Appl. Phys. A* **127**, 22 (2021).
23. J. He, Y. Qu, H. Li, J. Mi, and W. Ji, "Three-photon absorption in ZnO and ZnS crystals," *Opt. Express* **13**, 9235 (2005).
24. M. Heinemann and C. Heiliger, "Auger recombination rates in ZnMgO from first principles," *J. Appl. Phys.* **110**, 083103 (2011).
25. X. Zhang, W. Ji, and S. Tang, "Determination of optical nonlinearities and carrier lifetime in ZnO," *J. Opt. Soc. Am. B* **14**, 1951 (1997).
26. B. K. Meyer, H. Alves, D. M. Hofmann, W. Kriegseis, D. Forster, F. Bertram, J. Christen, A. Hoffmann, M. Straßburg, M. Dworzak, U. Haboeck, and A. V. Rodina, "Bound exciton and donor-acceptor pair recombinations in ZnO," *Phys. Status Solidi B* **241**, 231 (2004).
27. W. A. Tisdale, M. Muntwiler, D. J. Norris, E. S. Aydil, and X. Zhu, "Electron dynamics at the ZnO (10 $\bar{1}$ 0) surface," *J. Phys. Chem. C* **112**, 14682 (2008).
28. Y. Zhang, Q. Jiang, K. Cao, T. Chen, K. Cheng, S. Zhang, D. Feng, T. Jia, Z. Sun, and J. Qiu, "Extremely regular periodic surface structures in a large area efficiently induced on silicon by temporally shaped femtosecond laser," *Photonics Res.* **9**, 839 (2021).
29. D. Dufft, A. Rosenfeld, S. K. Das, R. Grunwald, and J. Bonse, "Femtosecond laser-induced periodic surface structures revisited: a comparative study on ZnO," *J. Appl. Phys.* **105**, 034908 (2009).
30. T. Jia, F. Zhao, M. Huang, H. Chen, J. Qiu, R. Li, Z. Xu, and H. Kuroda, "Alignment of nanoparticles formed on the surface of 6H-SiC crystals irradiated by two collinear femtosecond laser beams," *Appl. Phys. Lett.* **88**, 111117 (2006).
31. S. Höhm, A. Rosenfeld, J. Krüger, and J. Bonse, "Area dependence of femtosecond laser-induced periodic surface structures for varying band gap materials after double pulse excitation," *Appl. Surf. Sci.* **278**, 7 (2013).
32. T. Jia, H. Chen, M. Huang, F. Zhao, X. Li, S. Xu, H. Sun, D. Feng, C. Li, X. Wang, R. Li, Z. Xu, X. He, and H. Kuroda, "Ultraviolet-infrared femtosecond laser-induced damage in fused silica and CaF₂ crystals," *Phys. Rev. B* **73**, 054105 (2006).